LETTER • **OPEN ACCESS**

Modest ocean warming difference, explosive intensification: marine heatwave control of Typhoon Hagibis (2019)

To cite this article: Hwan-Young Choi *et al* 2026 *Environ. Res. Lett.* **21** 104013

ENVIRONMENTAL RESEARCH
LETTERS

OPEN ACCESS

RECEIVED
13 February 2026

REVISED
25 April 2026

ACCEPTED FOR PUBLICATION
30 April 2026

PUBLISHED
19 May 2026

LETTER

Modest ocean warming difference, explosive intensification: marine heatwave control of Typhoon Hagibis (2019)

Hwan-Young Choi[1,2], **Myung-Sook Park**[2,*], **Chaehyeon Chelsea Nam**[3], **Michael M Bell**[4] and **Hyeong-Seog Kim**[1,*]

[1] Ocean Science and Technology School, Korea Maritime and Ocean University, Busan, Republic of Korea
[2] Korea Ocean Satellite Center, Korea Institute of Ocean Science & Technology, Busan, Republic of Korea
[3] Department of Earth, Ocean and Atmospheric Sciences at Florida State University, Tallahassee, FL, United States of America
[4] Department of Atmospheric Science, Colorado State University, Fort Collins, CO, United States of America
[*] Authors to whom any correspondence should be addressed.

E-mail: mspark@kiost.ac.kr and hyeongseog@kmou.ac.kr

Keywords: marine heat waves, explosive rapid intensification, subsurface ocean heat content

Supplementary material for this article is available online

Abstract

Typhoon Hagibis (2019) explosively intensified by 100 kt in 24 h, greatly exceeding the conventional rapid intensification (RI) threshold of ∼30 kt per 24 h. This study investigates how marine heatwave (MHW)-driven ocean surface and subsurface structures influence such explosive RI (ERI). Using the coupled Weather Research and Forecasting and 3D Price–Weller–Pinkel Ocean model, we compared a Hagibis control run with two sensitivity experiments using non-MHW sea surface temperatures (SSTs) and vertical temperature profiles from another RI case of Typhoon Jebi (2018). Hagibis intensifies dramatically faster under MHW conditions—about 20% faster in the baseline simulation, and 40% faster when realistic vertical ocean mixing in the surface layer is included—revealing the striking sensitivity of ERI to upper-ocean thermal anomalies. Strong latent heat fluxes supplied continuous energy to the lower troposphere, while elevated subsurface heat content sustained air–sea enthalpy exchange despite storm-induced SST cooling. These ocean–atmosphere interactions reorganized TC convection, strengthened updrafts, and fostered an environment conducive to ERI. We conclude that even a 1 °C increase in surface temperature is sufficient to modulate storm structure and intensity, amplifying ERI. As ocean temperatures continue to rise, these findings highlight the need to refine the definition of ERI and improve our understanding of TC-ocean interactions under increasing MHW influence.

1. Introduction

Rapid intensification (RI), defined as a ⩾30 kt increase in maximum wind speed within 24 h (Kaplan and DeMaria 2003), is one of the most significant and unpredictable stages in the evolution of tropical cyclones (TCs). Under a warming climate, the frequency of RI events has increased over the past decades (Song *et al* 2020, Klotzbach *et al* 2022, Li *et al* 2023), yet several historical storms have strengthened at rates far beyond the conventional RI threshold. In 24 h, Hurricane Wilma (2005) intensified by nearly 95 kt, Hurricane Patricia (2015) strengthened by over 105 kt, and Typhoon Hagibis (2019) increased by approximately 100 kt. Such exceptional cases are often referred to as extreme or explosive RI (hereafter, ERI; e.g. Hendricks *et al* 2010, Kaplan *et al* 2015, Chen *et al* 2023), highlighting a distinct upper tail of intensification that typical RI processes may not fully explain. Favorable conditions for RI, such as warm sea Surface temperature (SST) (Lin *et al* 2009, Xu and Wang 2018), high ocean heat content (Chih and Wu 2020, Pun *et al* 2023), weak vertical shear (Frank and Ritchie 2001, Tao and Zhang 2015), and a moist mid-troposphere (Kaplan *et al* 2010, Rogers *et al* 2013, 2017), are well known, but they do not fully explain ERI. This motivates examining whether anomalously high SSTs associated with marine heatwaves (MHWs; Hobday *et al* 2016) can effectively act as a primary amplifier of ERI.

MHWs have been linked to stronger TC intensification. Observed cases include Hurricane Michael

(2018), which intensified over an MHW that limited SST cooling (Dzwonkowski *et al* 2020), and TC Amphan (2020), which strengthened over anomalously high heat content (Rathore *et al* 2022). A recent multi-case study further showed that TCs crossing MHW regions intensified ∼35% more than non-MHW cases in the western North Pacific and Atlantic (Choi *et al* 2024), highlighting enhanced latent heat flux (LHF) and concentrated precipitation near the core as key drivers. MHWs enhance surface enthalpy fluxes that fuel deep convection and vortical hot towers (Montgomery *et al* 2006, Fierro *et al* 2009). While MHWs are known to favor RI, their role in driving ERI remains unclear, underscoring the need to assess how MHW anomalies enable such extremes.

Typhoon Hagibis (2019) represents an ERI TC that crossed an MHW region. Developing on 6 October 2019, Hagibis rapidly intensified from a tropical storm (60 kt) to category 5 strength (160 kt) within 24 h, marking one of the most extreme ERI events on record. After reaching its lifetime maximum intensity (LMI) near the Mariana Islands, the storm tracked north-westward and made landfall over Japan. A useful contrast is provided by Typhoon Jebi (2018), which followed a similar large-scale track but intensified at roughly half the rate (∼50 kt per 24 h) and did not traverse a MHW region. To quantify oceanic control on ERI, we conducted sensitivity experiments for Hagibis by prescribing non-MHW ocean conditions based on Typhoon Jebi (2018), isolating the role of upper-ocean thermal structure. Lin *et al* (2021) analyzed Hagibis (2019) and Haiyan (2013), showing how multiscale environmental factors, including ocean heat content and translation speed, led to their contrasting intensity evolutions. Here, we extend this framework by using a coupled atmosphere–ocean model to quantify how MHW-related surface warming and subsurface heat reservoirs influenced Hagibis's explosive RI, thereby revealing the ocean–atmosphere processes that enabled this event.

2. Materials & methods

2.1. Data and methods

We used the Joint Typhoon Warning Center (JTWC) best track data, which provided 6-hourly TC center positions and maximum wind speeds. Daily SST data were obtained from the NOAA 1/4° Optimum Interpolation Sea Surface Temperature (NOAA OISST) dataset. MHWs were identified following Hobday *et al* (2016) using a 90th percentile SST threshold over a 30 year climatology.

We examined upper-ocean temperature and salinity profiles in the Western North Pacific using data from the Argo program within a 10° radius of each TC center, 48 h before RI (figure S1(a)). Although Argo data along the TC tracks were limited, we extracted profiles by averaging two Argo observations within the TC's spatial domain for each case. The SST values from these profiles were consistent with OISST, and the temperature-salinity structures agreed well with GLORYS12 reanalysis (figure S1(b)), confirming their reliability for representing oceanic conditions during TC passage.

To derive atmospheric environmental parameters, including vertical wind shear (VWS) and relative humidity, we used the NCEP Climate Forecast System Reanalysis (Version 2) dataset at 6-hourly intervals, with a 1° spatial resolution. We calculated VWS as the difference between the mean vector winds at 850 and 200 hPa over a 200–800 km radius ring around the TC center (DeMaria *et al* 2005). We calculated relative humidity as the mean over the same region's 500–700 hPa layer. We computed tropical cyclone heat potential (TCHP), defined as the integrated ocean heat content above the 26 °C isotherm, following the method of Leipper and Volgenau (1972). TCHP values were averaged within a 2° × 2° box centered on the storm position during the 48 h preceding the onset of RI.

2.2. Model description

We used the Advanced Research Weather Research and Forecasting (ARW-WRF) Model, version 4.4.2 (Skamarock *et al* 2019), to simulate interactions between TC and the ocean under the MHW conditions. The WRF model handled atmospheric processes, while the three-dimensional Price–Weller–Pinkel (3DPWP) Ocean model simulated how the mixed layer evolves due to entrainment mixing and air–sea exchanges (Price *et al* 1986, 1994). The 3DPWP model represents upper-ocean cooling processes during TC passage, including vertical mixing, upwelling, horizontal advection, and air–sea heat exchange (Srinivas *et al* 2016, Wu *et al* 2016). As an extension of the one-dimensional PWP model, the 3DPWP framework incorporates horizontal advection to represent upper-ocean evolution better while retaining the mixed-layer physics that govern the ocean response to TC forcing. The coupled WRF 3DPWP system used a triple-nested domain setup, in which the ocean model shares the same horizontal grid structure and resolutions as the atmospheric model. The outer, middle, and inner domains covered 140°E–150°E and 10°N–20°N, with horizontal resolutions of 9 km, 3 km, and 1 km, respectively. The atmospheric model used 50 vertical levels, with a top at 50 hPa. In addition, the ocean model had 30 vertical layers, organized as follows: 5 m intervals from 5 to 105 m, 10 m intervals from 115 to 195 m, and 20 m intervals from 210 to 390 m.

The atmospheric model included the WSM6-class Graupel microphysics scheme (Hong and Lim 2006), the RRTM longwave radiation scheme (Mlawer *et al* 1997), and the Dudhia shortwave radiation scheme (Dudhia 1989). The Yonsei University planetary

boundary layer scheme (Hong and Lim 2006, Hong 2010) was employed, with surface fluxes calculated using the Monin–Obukhov scheme and land processes represented by the Unified NOAH Land Surface Model. Cumulus convection was parameterized with the Kain–Fritsch scheme (Kain 2004) in the 9 km outer domain, while no cumulus parameterization was used in the 3 km and 1 km nested domains, where convection is explicitly resolved at sufficiently high resolution.

3. Model experimental design

3.1. Contrasting ocean and atmosphere conditions of Hagibis and Jebi

Typhoons Hagibis (2019) and Jebi (2018) represent RI TCs that developed over warm waters favorable for RI, yet their intensity evolution diverged markedly (figure 1(b)): Hagibis intensified at roughly twice the rate of Jebi (100 vs. 50 kt per 24 h). Notably, the atmospheric environment was not more favorable for Hagibis. Hagibis (2019) experienced higher VWS (9–10 m s^{-1}) than Jebi (6–8 m s^{-1}), but their mid-level relative humidity was comparable (∼55%–56% vs. ∼53%–54%) (figures 1(c) and (d)). At the onset of RI, Jebi developed over SSTs of ∼29.2 °C, sufficient for intensification but not surpassing the MHW threshold, whereas Hagibis exceeded 30 °C, associated with a pronounced MHW (figures 1(e) and (f)). MHW conditions are characterized by elevated SST, containing a larger subsurface heat reservoir (Jebi: ∼70 kJ cm^{-2}, Hagibis: ∼160 kJ cm^{-2}).

3.2. Hypothesis and design of sensitivity experiments

To separate the effects of sea surface forcing and vertical ocean thermal structure on Hagibis's ERI from atmospheric forcing, we conducted four experiments: two using the WRF atmospheric-only model configuration and two employing the fully coupled WRF–3DPWP model (table 1). All simulations used identical atmospheric conditions to reproduce Hagibis but differed in their prescribed SST fields and vertical ocean temperature profiles. Initial and boundary conditions for the atmospheric model in all four experiments were from the NCEP Global Forecast System with 6-hourly temporal and 0.25° spatial resolutions. Ensemble simulations incorporated random moisture perturbations in the initial water vapor mixing ratio field below 950 hPa, ranging from −0.5 to 0.5 g kg^{-1} (Zhang and Tao 2013, Judt *et al* 2016, Nam *et al* 2023). Each experiment consisted of five ensemble members, and we used ensemble-mean values for cross-experiment comparisons. The control experiment (CTRL) used the observed MHW SST field during Hagibis's development. The non-MHW experiment (non-MHW) used the cooler SST pattern associated with Typhoon Jebi (2018). To isolate subsurface effects, the vertical-profile experiment (Vprof) used the CTRL SST while prescribing Argo-derived temperature profiles near the RI region, applied as horizontally homogeneous vertical profiles across the model domain. The combined experiment (non-MHW + Vprof) applied both the non-MHW SST and the Jebi-like vertical ocean temperature profile derived from Argo observations. CTRL and non-MHW use the atmosphere-only WRF model with prescribed SST and without ocean feedback, whereas Vprof and non-MHW + Vprof use the coupled WRF–3DPWP system with interactive SST and explicit ocean feedback. Although the ensemble size is small, the responses were consistent across members with minimal spread, indicating that the results reflect systematic oceanic influences rather than stochastic variability.

We assessed the performance of the CTRL to verify the model's ability to reproduce the observed track and intensity of Hagibis. The TC track and intensity of CTRL were evaluated using the JTWC best track data (figure S2). Numerical models have persistent difficulty capturing ERI—an exceptionally rare subset of RI events—because forecast systems tend to regress toward climatology and therefore systematically underestimate both RI and rapid weakening (Trabing and Bell 2020). Previous high-resolution studies highlight similar limitations: WRF simulations of Hurricane Patricia (2015) accurately reproduced the track but failed to capture its explosive intensification in the control configuration, while ERI was reproduced after assimilating extensive dropsonde and radar observations (Tao *et al* 2022). Consistent with these challenges, a 2 km configuration underestimated both the RI rate and LMI of Hagibis (figure S2). Increasing horizontal resolution to 1 km substantially improved the representation of ERI, yielding a more realistic evolution of the inner core intensification and convective organization, though it still underestimated the observed LMI and RI rate. Despite these biases, the model simulations reproduce the essential structure evolution and intensity tendency of Hagibis (figure 2), providing a physically credible framework for isolating the oceanic mechanisms through which MHW conditions promote ERI.

4. Impacts of MHWs on Hagibis ERI

4.1. Role of surface heating and subsurface structure in modulating ERI

TCs crossing MHW regions generally reach higher LMI than those over non-MHW environments (Dzwonkowski *et al* 2020, Rathore *et al* 2022, Choi *et al* 2024). Consistent with these studies, our experiments show significantly stronger LMIs in MHW experiments (Mann–Whitney U test, $p = 0.008$). When considering SST only, CTRL reaches an LMI

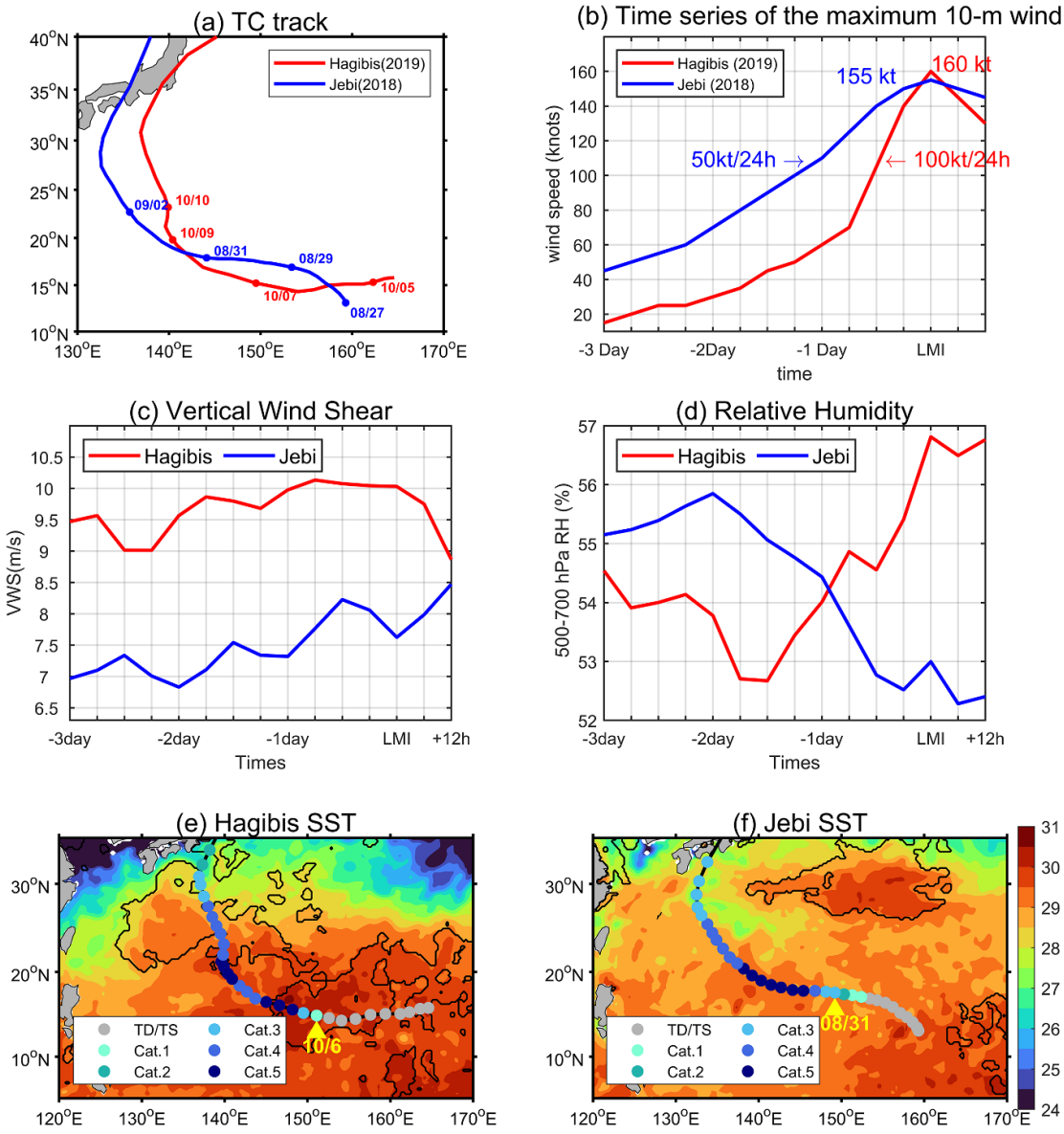

Figure 1. Background environment of TC development. (a) TC tracks, with selected date labels shown along the tracks for reference. (b) Time series of the maximum 10 m wind from JTWC, (c) vertical wind shear (VWS), and (d) mid-level relative humidity (RH). The *x*-axis shows time relative to the lifetime maximum intensity (LMI). (e)–(f) Pre-TC SST (2 d before RI, °C) for Hagibis and Jebi. Black contours indicate MHW regions. Yellow triangles mark the location and date of RI onset. Circles denote the TC track, with circle color representing TC intensity.

18% higher than the non-MHW experiment. When vertical ocean structure is also included, Vprof exceeds non-MHW + Vprof by 22% (figure 2(b)). Despite only ∼1 °C mean SST difference during the RI period, these pronounced LMI differences demonstrate the role of MHW conditions in determining TC maximum intensity.

TCs traversing MHW regions exhibit not only stronger LMI but also faster RI in our experiments. During the observed RI phase of Hagibis (6–7 October 2019), the model reproduced RI in all four experiments, though at lower rates than the observed 100 kt per 24 h. RI rates were consistently higher in MHW runs: CTRL intensified 20% (∼12 kt per 24 h) faster than the non-MHW case, and Vprof was ∼22 kt per 24 h faster than non-MHW + Vprof—an ∼41% enhancement associated with differences in upper-ocean structure (figure 2(c)). These results show that MHW conditions regulate not only the maximum intensity but also the rate of intensification, with subsurface thermal structure further amplifying this effect.

A comparison between the SST-only and mixing experiments reveals a stronger ocean-feedback contrast under MHW versus non-MHW conditions. CTRL represents an idealized simulation without ocean feedback, as SST is prescribed as a fixed initial OISST field at the onset of Hagibis and is not updated during the simulation; thus, storm-induced cooling is not represented. Although CTRL produces stronger peak intensity, this does not necessarily indicate a more realistic representation, as the

Table 1. List of experiments with corresponding experimental setups.

Experiment name	Description	TC case	SST	Vertical ocean profile (3DPWP)
Control run (CTRL)	Hagibis's observed SST with MHW	Hagibis	OISST(Hagibis)	×
Non-MHW experiment (non-MHW EXP)	Hagibis with non-MHW EXP forcing (removing MHW condition)	Hagibis	OISST(Jebi)	×
Vertical-profile experiment (Vprof EXP)	CTRL-EXP with MHW, but a simplified MHW vertical profile applied	Hagibis	OISST(Hagibis)	Argo (Hagibis)
Non-MHW + Vertical-profile experiment (non-MHW + Vprof EXP)	Hagibis with non-MHW EXP forcing (non-MHW) and simplified non-MHW vertical profile	Hagibis	OISST(Jebi)	Argo (Jebi)

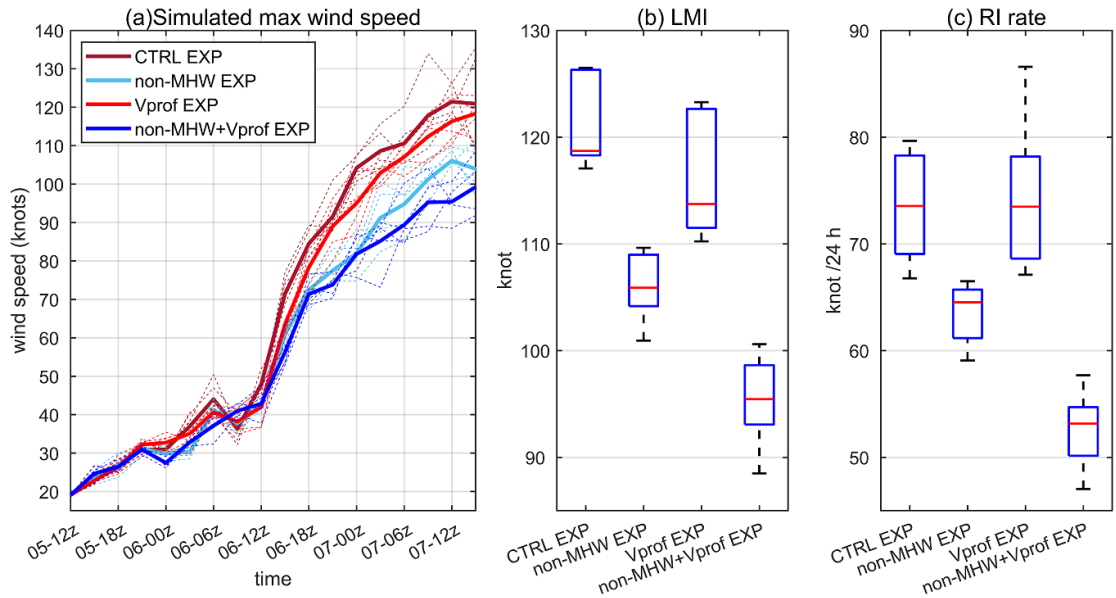

Figure 2. Simulated 10 m maximum wind speed and TC evolution with different ocean features in MHW. (a) The solid line represents the ensemble's mean 10 m maximum wind speed, while the dashed lines denote individual ensemble members. The dark red line corresponds to the CTRL, the sky-blue line represents the non-MHW EXP, the red line indicates the Vprof EXP, and the blue line denotes the non-MHW + Vprof EXP. (b) A box plot for each experiment's LMI (knots) values. (c) A box plot illustrates each experiment's RI rate (knots/24 h).

absence of ocean feedback can artificially sustain surface fluxes. Therefore, differences between CTRL and Vprof reflect the combined effects of ocean feedback processes and upper-ocean thermal structure. Under MHW conditions (CTRL vs. Vprof), vertical mixing produced only minor changes, reducing the LMI by ∼5 kt and the RI rate by 0.8 kt per 24 h, indicating a weak sensitivity of storm intensity to vertical mixing. In contrast, mixing exerted a much stronger suppressive effect in the non-MHW experiments, indicating a higher sensitivity of storm intensity to ocean feedback processes. The non-MHW + Vprof run yielded an ∼8% (∼8 kt) weaker storm and a 17% (∼9 kt per 24 h) slower RI rate than the non-MHW. Notably, when Hagibis's atmospheric forcing was applied to Jebi's ocean thermal structure (non-MHW + Vprof), the simulated RI rate (52.5 kt per 24 h) closely matched Jebi's observed intensification (50 kt per 24 h).

These results indicate that vertical mixing operates in two distinct regimes. Under MHW conditions, its influence is limited because the deep subsurface heat reservoir buffers storm-induced cooling. In contrast, under non-MHW conditions, where there is less upper-ocean heat available to support TC intensification, mixing acts as a primary constraint by depleting available oceanic heat. This mechanism aligns with previous findings that elevated TCHP buffers the impact of mixing-induced cooling and weakens negative intensity feedback (Lin *et al* 2003, Wada and Usui 2007, Halliwell *et al* 2015). To further assess the role of oceanic processes, translation speed and storm size were comparable across all experiments (table S1), suggesting that differences in intensification are

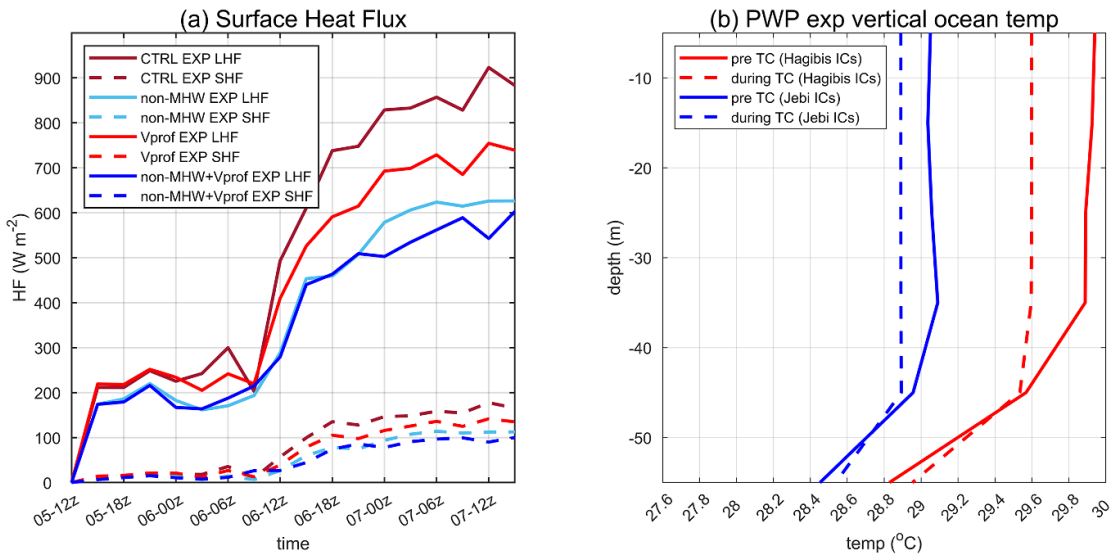

Figure 3. Air–sea interaction induced by RI TC. (a) Spatially averaged surface heat flux within a 2-degree radius of the TC center. Solid lines represent the latent heat flux, while dashed lines indicate the sensible heat flux for each experiment. (b) Vertical ocean temperature profiles before and after RI. solid lines represent the initial upper-ocean temperature profiles derived from Argo observations used as initial conditions (ICs) in the model (as described in table 1), while dashed lines show the simulated temperature profiles after RI from the coupled WRF–3DPWP experiments. Red and blue lines correspond to experiments initialized with Hagibis and Jebi ocean conditions, respectively.

not driven by storm dynamics but are associated with oceanic conditions under MHW.

4.2. Surface fluxes and ocean–atmosphere coupling

Previous studies have primarily focused on ocean-only controls (Xu and Wang 2018, Chih and Wu 2020) or atmospheric factors (Tao and Zhang 2015, Rogers *et al* 2017). Here, we provide a perspective by investigating how anomalous ocean states with MHWs and ocean–atmosphere coupling jointly reorganize convective structure and accelerate ERI.

Surface heat fluxes, which exchange momentum and moist enthalpy between the ocean and the atmosphere, play a central role in modulating TC intensity (Gao and Chiu 2010, Gao *et al* 2016). Figure 3 shows that enhanced surface enthalpy fluxes were characterized by MHW experiments, with latent and sensible heat fluxes 36%–51% higher than in non-MHW cases. LHF dominated the exchange, exceeding sensible heat flux by approximately a factor of six.

Our results suggest a mechanism whereby subsurface ocean heat content influences air–sea fluxes through its control on SST cooling. Under MHW conditions, despite SST cooling of ∼0.34 °C (figure 3(b)), elevated pre-RI TCHP (113.6 kJ cm^{-2}) appears to buffer this cooling and sustain surface enthalpy fluxes, supporting continued intensification. In contrast, lower initial TCHP in non-MHW cases (88.3 kJ cm^{-2}) leads to stronger cooling, reduced fluxes, and weaker intensification (∼52 kt per 24 h). These results are consistent with previous findings that reduced upper-ocean heat content amplifies storm-induced cooling and constrains intensification (Lin *et al* 2009, Wang *et al* 2016).

We analyzed model-simulated radar reflectivity to assess how enhanced surface enthalpy flux under MHW conditions sustains convective processes critical to TC development and intensification. To capture the distribution of convective structures, we employed contoured frequency by altitude diagrams (CFADs; Yuter & Houze 1995) of vertical motion and reflectivity within a 2° radius from the TC center, representing inner-core convective regions and normalized against the multi-experiment mean. CFADs were used to highlight differences in the frequency and vertical organization of convective features, thereby revealing how latent heating and cooling evolved during the RI period (Rogers *et al* 2007, 2010, Onderlinde and Nolan 2016).

CFADs of reflectivity reveal that anomalies at 10–20 dBZ correspond to stratiform precipitation, while those exceeding 30 dBZ indicate convective bursts (Rogers *et al* 2007, Park *et al* 2017). MHW TCs exhibit pronounced positive anomalies within 30–40 dBZ and stronger updrafts, highlighting the prevalence of deep convection (figures 4(b) and (d)). Sustained surface enthalpy fluxes under MHW conditions are associated with enhanced deep convection. These results indicate that MHWs buffer the negative feedback associated with storm-induced SST cooling, allowing intense convection to support ERI.

The CFAD analysis shows that MHW conditions alter the inner-core structure. In CTRL, reflectivity is concentrated in the lower troposphere (1–4 km), indicating a warm-rain regime. When the subsurface MHW structure is included (Vprof), reflectivity shifts upward, with enhanced signals in the mid- to upper troposphere. This upward shift

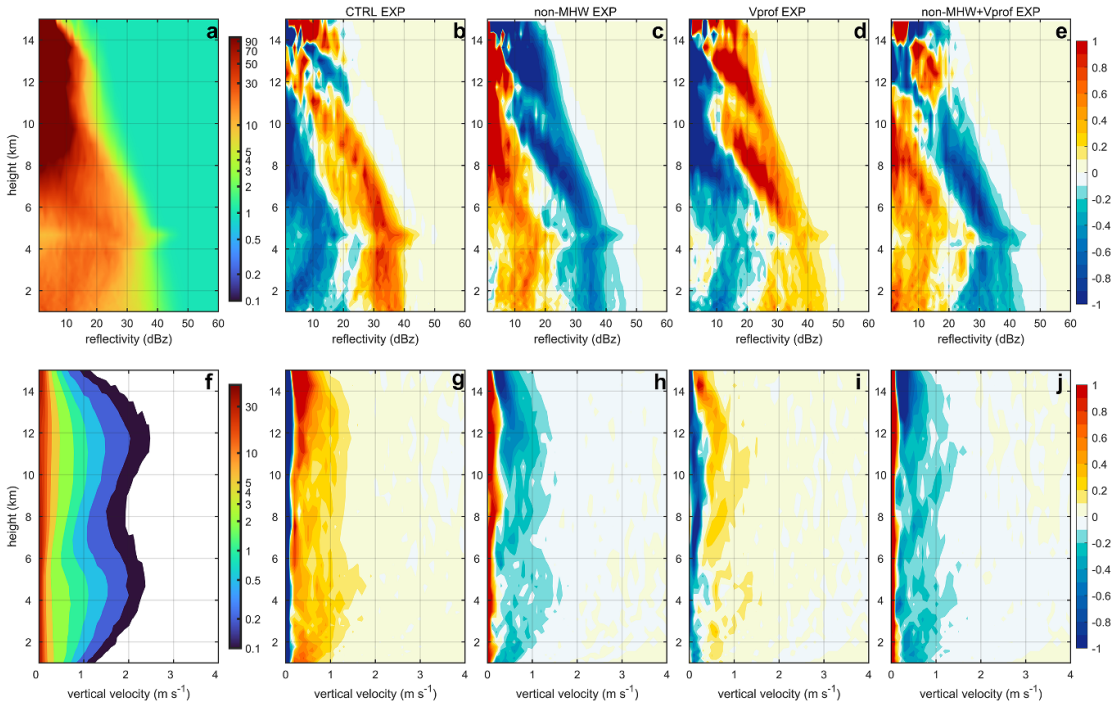

Figure 4. Vertical structure of TC with CFAD. Simulated CFADs of radar reflectivity (first row) and vertical velocity (second row). (a) and (f) Show the mean radar reflectivity CFAD and vertical velocity for 6 October 2015–18 UTC across all four experiments. (b)–(e) Displays the radar reflectivity anomalies relative to the mean for each experiment, while (g)–(j) shows the vertical velocity anomalies. The second column corresponds to the CTRL-EXP experiment, the third to the non-MHW EXP experiment, the fourth to the Vprof EXP experiment, and the fifth to the non-MHW + Vprof EXP experiment.

reflects stronger mid-level updrafts and more efficient vertical transport of hydrometeors, leading to deeper, more organized convection that reinforces ERI. This difference highlights the role of ocean feedback: including subsurface structure allows SST cooling to interact with the storm, resulting in a more physically consistent representation of convective evolution.

These findings show that MHW conditions enhance surface enthalpy fluxes, invigorate inner-core convection, and sustain air–sea energy exchange despite storm-induced cooling, driven by elevated TCHP. These results demonstrate a continuous physical pathway from enhanced subsurface heat content to sustained fluxes and deeper convection, which ultimately supports ERI. These processes emphasize the importance of representing subsurface thermal structure in RI prediction, particularly in a warming climate where MHWs are becoming more frequent.

5. Conclusion

ERI represents one of the most hazardous and devastating phases of the TC lifecycle, which can lead to catastrophic societal and economic impacts. By examining Category 5 Typhoon Hagibis (2019), we demonstrate the crucial role of the upper-ocean environment in controlling ERI. Even a modest ~1 °C warming beyond the MHW threshold accelerates intensification, with the CTRL experiment producing a 19.5% faster RI rate and 17.5% stronger LMI compared to the non-MHW experiment. These findings underscore the sensitivity of ERI to oceanic thermal anomalies. In particular, the role of subsurface ocean structure becomes even clearer when vertical profiles are included. Under the Vprof experiment, Hagibis intensifies 41.4% faster and reaches 21.9% higher LMI than in the non-MHW + Vprof experiment (figure 2). MHW conditions enhance air–sea enthalpy fluxes by 36%–51% (figure 3(a)), energizing the lower troposphere and strengthening deep convection, as reflected in increased 30–40 dBZ reflectivity and enhanced updrafts (figure 4). While the non-MHW cases experience negative feedback from storm-induced SST cooling, the initially elevated TCHP (~113 kJ cm^{-2}) within the MHW region buffers the thermodynamic impact of this cooling (figure 3(b)), enabling sustained storm growth.

These results provide a process-based explanation for why ERI arises from the coupled evolution of ocean and atmosphere. Consistent with previous studies highlighting subsurface heat content (Rathore *et al* 2022) and surface flux enhancement (Pun *et al* 2023) under MHW conditions, we show that MHW-associated subsurface warming sustains air–sea enthalpy fluxes and convective

organization by limiting storm-induced SST cooling, whereas stronger cooling suppresses intensification in non-MHW environment. This highlights the co-evolution of oceanic heat-content variability and atmospheric convective structure during explosive intensification. This integrated perspective links surface heat fluxes, subsurface ocean structure, and storm-internal convective dynamics within a unified framework. While this study focuses on MHW-driven subsurface effects, additional processes—such as sea-spray–mediated flux enhancement (Yang *et al* 2024, 2025), upper-ocean stratification (Balaguru *et al* 2020) and warm-core eddies (Ma *et al* 2021)—may also contribute to RI predictability, underscoring the importance of considering multiple ocean–atmosphere interaction pathways.

Hagibis ranks within the top 1% (99th percentile, see supplementary figure S3) of RI rates in the western North Pacific (1982–2023), supporting its classification as an ERI event. As MHWs become more frequent, intense, and persistent under anthropogenic warming (Oliver *et al* 2018), their influence on TC intensification may become more pronounced, particularly when accompanied by elevated subsurface heat content that can sustain air–sea energy exchange. Improving prediction of such high-impact events will require models that explicitly resolve coupled ocean–atmosphere feedbacks and take into account subsurface ocean structure.

Our experimental design does not fully isolate subsurface thermal structure under identical SST conditions; therefore, differences between experiments reflect the combined effects of ocean feedback and vertical thermal structure rather than subsurface heat content alone. Future experiments that isolate vertical thermal structure under identical SST conditions would further clarify the independent role of subsurface heat content.

Acknowledgments

This research was supported by the National Research Foundation of Korea (NRF) grant funded by the Korean government (MSIT) (2021R1A2C1014608 and RS-2025-24534063). This study was also supported by the Korea Institute of Marine Science and Technology Promotion (KIMST), funded by the Ministry of Oceans and Fisheries (20220566). MMB was supported under Office of Naval Research Awards N00014-20-1-2069 and N00014-24-1-2554.

Data availability statement

NOAA 1/4° daily Optimum Interpolation Sea Surface Temperature (OISST) data are available at https://psl.noaa.gov/data/gridded/data.noaa.oisst.v2.highres.html. Tropical cyclone best track data are provided by the Joint Typhoon Warning Center (JTWC) (www.metoc.navy.mil/jtwc/jtwc.html?best-tracks). Vertical ocean temperature data are obtained from the Argo program (https://dataselection.euro-argo.eu/) and the GLORYS ocean reanalysis (https://data.marine.copernicus.eu/products).

The WRF–3DPWP model configuration and experimental setup are described in the Methods section. Model output data and analysis scripts supporting the findings of this study are available from the corresponding author upon reasonable request.

Supplementary Figures S1–S3 available at https://doi.org/10.1088/1748–9326/ae6713/data1.

ORCID iDs

Hwan-Young Choi 0009-0000-4128-9507
Myung-Sook Park 0000-0003-1262-7786
Chaehyeon Chelsea Nam 0000-0002-3607-7523
Michael M Bell 0000-0002-0496-331X
Hyeong-Seog Kim 0000-0003-2577-3301

References

Balaguru K, Foltz G R, Leung L R, Kaplan J, Xu W, Reul N and Chapron B 2020 Pronounced impact of salinity on rapidly intensifying tropical cyclones *Bull. Am. Meteorol. Soc.* **101** E1497–E511

Chen B F, Kuo Y T and Huang T S 2023 A deep learning ensemble approach for predicting tropical cyclone rapid intensification. Atmos *Sci. Lett.* **24** e1151

Chih C H and Wu C C 2020 Exploratory analysis of upper-ocean heat content and sea surface temperature underlying tropical cyclone rapid intensification in the western North Pacific *J. Clim.* **33** 1031–50

Choi H Y, Park M S, Kim H S and Lee S 2024 Marine heatwave events strengthen the intensity of tropical cyclones *Commun. Earth Environ.* **5** 69

DeMaria M, Mainelli M, Shay L K, Knaff J A and Kaplan J 2005 Further improvements to the statistical hurricane intensity prediction scheme (SHIPS) *Weather Forecast.* **20** 531–43

Dudhia J 1989 Numerical study of convection observed during the winter monsoon experiment using a mesoscale two-dimensional model *J. Atmos. Sci.* **46** 3077–107

Dzwonkowski B, Coogan J, Fournier S, Lockridge G, Park K and Lee T 2020 Compounding impact of severe weather events fuels marine heatwave in the coastal ocean *Nat. Commun.* **11** 4623

Fierro A O, Rogers R F, Marks F D and Nolan D S 2009 The impact of horizontal grid spacing on the microphysical and kinematic structures of strong tropical cyclones simulated with the WRF-ARW model *Mon. Weather Rev.* **137** 3717–43

Frank W M and Ritchie E A 2001 Effects of vertical wind shear on the intensity and structure of numerically simulated hurricanes. Mon *Weather Rev.* **129** 2249–69

Gao S and Chiu L S 2010 Surface latent heat flux and rainfall associated with rapidly intensifying tropical cyclones over the western North Pacific *Int. J. Remote Sens.* **31** 4699–710

Gao S, Zhai S, Chiu L S and Xia D 2016 Satellite air–sea enthalpy flux and intensity change of tropical cyclones over the western North Pacific *J. Appl. Meteorol. Climatol.* **55** 425–44

Halliwell G R, Gopalakrishnan S, Marks F and Willey D 2015 Idealized study of ocean impacts on tropical cyclone intensity forecasts *Mon. Weather Rev.* **143** 1142–65

Hendricks E A, Peng M S, Fu B and Li T 2010 Quantifying environmental control on tropical cyclone intensity change. Mon *Weather Rev.* **138** 3243–71
Hobday A J *et al* 2016 A hierarchical approach to defining marine heatwaves *Prog. Oceanogr.* **141** 227–38
Hong S Y 2010 A new stable boundary-layer mixing scheme and its impact on the simulated East Asian summer monsoon *Q. J. R. Meteorol. Soc.* **136** 1481–96
Hong S Y and Lim J O J 2006 A new vertical diffusion package with an explicit treatment of entrainment processes *Asia-Pac. J. Atmos. Sci.* **42** 129–51
Judt F, Chen S S and Berner J 2016 Predictability of tropical cyclone intensity: scale-dependent forecast error growth in high-resolution stochastic kinetic-energy backscatter ensembles *Q. J. R. Meteorol. Soc.* **142** 43–57
Kain J S 2004 The Kain–Fritsch convective parameterization: an update *J. Appl. Meteorol.* **43** 170–81
Kaplan J *et al* 2015 Evaluating environmental impacts on tropical cyclone rapid intensification predictability utilizing statistical models *Weather Forecast.* **30** 1374–96
Kaplan J and DeMaria M 2003 Large-scale characteristics of rapidly intensifying tropical cyclones in the North Atlantic basin *Weather Forecast.* **18** 1093–108
Kaplan J, DeMaria M and Knaff J A 2010 A revised tropical cyclone rapid intensification index for the Atlantic and eastern North Pacific basins *Weather Forecast.* **25** 220–41
Klotzbach P J, Wood K M, Schreck C J, Bowen S G, Patricola C M and Bell M M 2022 Trends in global tropical cyclone activity: 1990–2021 *Geophys. Res. Lett.* **49** e2021GL095774
Leipper D F and Volgenau D 1972 Hurricane heat potential of the Gulf of Mexico *J. Phys. Oceanogr.* **2** 218–24
Li Y, Tang Y, Wang S, Toumi R, Song X and Wang Q 2023 Recent increases in tropical cyclone rapid intensification events in global offshore regions *Nat. Commun.* **14** 5167
Lin I I *et al* 2021 A tale of two rapidly intensifying supertyphoons: Hagibis (2019) and Haiyan *Bull. Am. Meteorol. Soc.* **102** E1645–64
Lin I I, Chen C H, Pun I F, Liu W T and Wu C C 2009 Warm ocean anomaly, air–sea fluxes, and the rapid intensification of tropical cyclone Nargis (2008) *Geophys. Res. Lett.* **36** L03817
Lin I I, Liu W T, Wu C C, Chiang J C H and Sui C H 2003 Satellite observations of modulation of surface winds by typhoon-induced upper ocean cooling *Geophys. Res. Lett.* **30** 1150
Ma Z *et al* 2021 Imprints of tropical cyclones on structural characteristics of mesoscale oceanic eddies over the western North Pacific *Geophys. Res. Lett.* **48** e2021GL09260
Mlawer E J, Taubman S J, Brown P D, Iacono M J and Clough S A 1997 Radiative transfer for inhomogeneous atmospheres: RRTM, a validated correlated-k model for the longwave *J. Geophys. Res. Atmos.* **102** 16663–82
Montgomery M T, Nicholls M E, Cram T A and Saunders A B 2006 A vortical hot tower route to tropical cyclogenesis *J. Atmos. Sci.* **63** 355–86
Nam C C, Bell M M and Tao D 2023 Bifurcation points for tropical cyclone genesis and intensification in sheared and dry environments *J. Atmos. Sci.* **80** 2239–59
Oliver E C J *et al* 2018 Longer and more frequent marine heatwaves over the past century *Nat. Commun.* **9** 1324
Onderlinde M J and Nolan D S 2016 Tropical cyclone–relative environmental helicity and the pathways to intensification in shear *J. Atmos. Sci.* **73** 869–90
Park M S, Lee M-I, Kim D, Bell M M, Cha D-H and Elsberry R L 2017 Land-based convection effects on formation of tropical cyclone Mekkhala (2008) *Mon. Weather Rev.* **145** 1315–37
Price J F, Sanford T B and Forristall G Z 1994 Forced stage response to a moving hurricane *J. Phys. Oceanogr.* **24** 233–60
Price J F, Weller R A and Pinkel R 1986 Diurnal cycling: observations and models of the upper ocean response to diurnal heating, cooling, and wind mixing *J. Geophys. Res. Oceans* **91** 8411–27
Pun I F, Hsu H H, Moon I J, Lin I I and Jeong J Y 2023 Marine heatwave as a supercharger for the strongest typhoon in the East China Sea *Npj. Climate. Atmos. Sci.* **6** 128
Rathore S, Goyal R, Jangir B, Ummenhofer C C, Feng M and Mishra M 2022 Interactions between a marine heatwave and tropical cyclone Amphan in the Bay of Bengal in 2020 *Front. Clim.* **4** 861477
Rogers R F, Aberson S, Bell M M, Cecil D J, Doyle J D, Kimberlain T B, Velden C, Shay L K and Velden C 2017 Rewriting the tropical record books: the extraordinary intensification of Hurricane Patricia (2015) *Bull. Am. Meteorol. Soc.* **98** 2091–112
Rogers R F, Black M L, Chen S S and Black R A 2007 An evaluation of microphysics fields from mesoscale model simulations of tropical cyclones. Part I: comparisons with observations *J. Atmos. Sci.* **64** 1811–34
Rogers R F, Reasor P D and Lorsolo S 2013 Airborne Doppler observations of the inner-core structural differences between intensifying and steady-state tropical cyclones *Mon. Weather Rev.* **141** 2970–91
Rogers R 2010 Convective-scale structure and evolution during a high-resolution simulation of tropical cyclone rapid intensification *J. Atmos. Sci.* **67** 44–70
Skamarock W C *et al* 2019 A description of the advanced research WRF version 4 *NCAR Tech. Note NCAR/TN-556+STR*
Song J, Duan Y and Klotzbach P J 2020 Increasing trend in the rapid intensification magnitude of tropical cyclones over the western North Pacific *Environ. Res. Lett.* **15** 084043
Srinivas C V, Mohan G M, Naidu C V, Baskaran R and Venkatraman B 2016 Impact of air–sea coupling on the simulation of tropical cyclones in the North Indian Ocean using a simple 3-D ocean model coupled to ARW *J. Geophys. Res. Atmos.* **121** 9400–21
Tao D, Van Leeuwen P J, Bell M and Ying Y 2022 Dynamics and predictability of tropical cyclone rapid intensification in ensemble simulations of Hurricane Patricia (2015) *J. Geophys. Res. Atmos.* **127** e2021JD036079
Tao D and Zhang F 2015 Effects of vertical wind shear on the predictability of tropical cyclones: practical versus intrinsic limit *J. Adv. Model. Earth Syst.* **7** 1534–53
Trabing B C and Bell M M 2020 Understanding error distributions of hurricane intensity forecasts during rapid intensity changes *Weather Forecast.* **35** 2219–34
Wada A and Usui N 2007 Importance of tropical cyclone heat potential for tropical cyclone intensity and intensification in the western North Pacific *J. Oceanogr.* **63** 427–47
Wang G, Wu L, Johnson N C and Ling Z 2016 Observed three-dimensional structure of ocean cooling induced by Pacific tropical cyclones *Geophys. Res. Lett.* **43** 7632–8
Wu C C, Tu W T, Pun I F, Lin I I and Peng M S 2016 Tropical cyclone-ocean interaction in Typhoon Megi (2010)—a synergy study based on ITOP observations and atmosphere-ocean coupled model simulations *J. Geophys. Res. Atmos.* **121** 153–67
Xu J and Wang Y 2018 Dependence of tropical cyclone intensification rate on sea surface temperature, storm intensity, and size in the western North Pacific *Weather Forecast.* **33** 523–37
Yang S *et al* 2025 Sea spray effects on typhoon prediction in the Yellow and East China Seas: case studies using a coupled atmosphere–ocean–wave model for Lingling (2019) and Maysak *Environ. Res. Lett.* **20** 054028
Yang S, Shin D W, Cocke S, Nam C C, Bourassa M, Cha D-H and Kim B-M 2024 Unveiling the pivotal influence of sea spray heat fluxes on hurricane rapid intensification *Environ. Res. Lett.* **19** 114058
Yuter S E and Houze Jr R A 1995 Three-dimensional kinematic and microphysical evolution of Florida cumulonimbus. Part II: frequency distributions of vertical velocity, reflectivity, and differential reflectivity *Mon. Weather Rev.* **123** 1941–63
Zhang F and Tao D 2013 Effects of vertical wind shear on the predictability of tropical cyclones *J. Atmos. Sci.* **70** 975–83